Dental pulp stem cells-derived cannabidiol-pretreated micro-spheroids showed robust osteogenic potential via upregulation of WNT6

Fangqi Liu
Stomatology Hospital of Guangzhou Medical University
Qingqing Wu
Stomatology Hospital of Guangzhou Medical University
Qianwen Liu
Stomatology Hospital of Guangzhou Medical University
Bo Chen
Stomatology Hospital of Guangzhou Medical University
Xintong Liu
Janak Lal Pathak
Nobumoto Watanabe
Jiang Li (ljiang@gzhmu.edu.cn)
Stomatology Hospital of Guangzhou Medical University

Article

Keywords: Dental pulp stem cells, Cannabidiol, Osteogenic differentiation, Micro-spheroids, WNT6, Tissue engineering

Posted Date: March 1st, 2023

DOI: https://doi.org/10.21203/rs.3.rs-2580851/v1

Abstract

Dental pulp stem cells (DPSC)-derived 3D-aggregates/spheroids have shown robust soft/hard tissue regeneration potential. However, difficulties to control the cell number, size, and shape of DPSC-aggregates/spheroids cause cell necrosis and difficulties in homogenous seeding of aggregates/spheroids in the 3D-printed microporous bone grafts. Moreover, inducing the osteogenic potential of these aggregates/spheroids is still a challenge. This study developed cannabidiol (CBD)-pretreated, self-assembled, and injectable DPSC-derived osteogenic micro-spheroids (70 μm) that robustly promoted in situ bone regeneration. We developed micro-spheroids by seeding 250 cells/microwell in agarose gel microwells of 200 μm diameter developed using prefabricated mold and cultured with CBD for 14 days to induce osteogenic potential. In vitro study results showed that CBD did not affect the viability of DPSC but promoted osteogenic differentiation during 2D culture. In micro-spheroids, 3D cytoskeleton visualization showed better integrity and robustly higher expression of osteogenic markers and promoted in situ bone regeneration compared with DPSC. CBD-pretreated micro-spheroids showed robustly higher bone-regenerative capacity via upregulation of WNT6. Taken together, our approach of developing organoid-like injectable osteogenic micro-spheroids can be used as the effective carrier of the effect of in vitro drug treatment during in situ bone tissue engineering which eliminates the direct in vivo drug application-related adverse effects.

Introduction

Development of functional bone constructs using mesenchymal stem cells (MSCs), biomimetic biomaterial scaffolds, and growth factors are current strategies of bone tissue engineering (1–3). Autologous MSCs obtained from different anatomical sites such as bone marrow, adipose tissue, and dental pulp are commonly used in clinics to repair large-sized bone defects (4–6). Dental pulp stem cells (DPSC), as easily accessible MSCs, can be extracted from orthodontic teeth or wisdom teeth in a non-invasive way (4, 7). Due to easy accessibility, high proliferation ability, and multi-lineage differentiation properties, DPSC are considered of particular interest for orthopedic and oral maxillofacial reconstruction as well as for dental tissue regeneration in the last decades (8–10). However, the clinical outcomes of DPSC-based bone tissue-engineering strategies are still not satisfactory.

During stem cell-based bone tissue engineering, in vivo seeded MSCs should proliferate and survive long enough to differentiate in osteoblasts as well as to release the growth factors and chemokines to influence the cells of surrounding tissues such as endothelial cells and macrophages (11, 12). However, the grafted seed cells can survive only a few days in vivo fading effective bone regeneration (13, 14). Recent advances in 3D culture technology have developed MSC-derived cell sheets (15), micro-tissues, spheroids (16), and organoids (17, 18) that provide superior nutrient, oxygen gradients, cell-cell interaction, and matrix deposition required for tissue regeneration (19–21). 3D-printed porous bone grafts are mainly designed with pore sizes 200–500 μm (22). Cell aggregates/spheroids produced by the conventional 3D culture techniques fail to control the size and cell numbers which causes cell necrosis and difficulties in homogenous seeding of aggregates/spheroids throughout the micro-porous scaffolds

(13). Therefore, the use of the micro-well technique that can produce functional and injectable cell micro-spheroids with < 100 μm size could allow the seeding of spheroids homogeneously in microporous bone grafts during the surgical procedure (23).

Inducing the osteogenic potential of cell aggregates/spheroids during bone defect healing is still a challenge. Extracts from natural products have shown promising potential to promote bone regeneration (24, 25). Cannabidiol (CBD), a major non-psychotropic constituent of Cannabis sativa, promotes the osteogenic differentiation of DPSC (26). CBD has certain biological activities required for bone tissue engineering such as anti-inflammatory (27), antioxidant (28), chemotactic (29), angiogenic, and osteogenic (30) properties. However, whether CBD could promote the osteogenic potential of DPSC-derived micro-spheroids is still unknown. Although CBD is a relatively safe drug for in vivo application, it might still exert local and systemic adverse effects (31, 32). Therefore, inducing the DPSC micro-spheroids with CBD in vitro, instead of direct in vivo use of CBD, could eliminate the CBD-related adverse effect in vivo during bone regeneration.

Based on these facts, this study aimed to develop CBD-pretreated DPSC micro-spheroids as an effective source of osteogenic seed cells for bone tissue engineering. We developed self-assembled DPSC micro-spheroids of 70 μm size using the microwell culture technique. Micro-spheroids were cultured with the osteogenic medium in presence of CBD for 14 days and in vitro or in vivo osteogenic potential was compared with 2D expanded DPSC in similar culture conditions. The mechanism of CBD-induced osteogenic potential of the DPSC micro-spheroids was further investigated.

Material And Methods

Isolation and characterization of DPSC

The present study was approved by the Medical Ethical Committee of the Affiliated Stomatology Hospital of Guangzhou Medical University (No. JCYJ2022021), and all patients signed an informed consent form. The DPSC were all obtained from the human pulp tissue of premolars that were removed for orthodontic treatment in the Affiliated Stomatology Hospital of Guangzhou Medical University. Total 30 teeth from 20 patients (10 male, 10, female, 1-2 tooth/patient) were used for DPSC isolation. The inclusion criteria for teeth collection were the permanent teeth from 18 to 25-year-old patients without caries, periodontal disease, periapical lesion, and systemic inflammatory diseases. After extraction, the teeth' surface was washed with phosphate-buffered saline (PBS) (Gibco, USA) containing 4% penicillin/streptomycin (Gibco, USA) 2 times. The pulp tissues were gently separated from the root and crown within 4 h, minced with sterile scissors into 1-2 mm fragments, then digested with 3 mg/mL collagenase type I (Gibco, USA) and 4 mg/mL dispase (Gibco, USA) for 45 min at 37℃, and centrifuged at 1000 rpm for 5 min. The cells’ precipitation was resuspended using alpha-modified minimal essential media (α-MEM; Gibco, USA) containing 15% fetal bovine serum (FBS) (Gibco, USA) and 1% of penicillin/streptomycin, and cultured at 37℃ in an environment with 5% CO_2 with the medium replacement every 3 days. Upon reaching 80-90%

confluency, cells were collected with 0.25% trypsin-EDTA (Gibco, USA) and subcultured at a 1:3 ratio. DPSC between passages 2 to 5 were used in subsequent experiments.

Flow cytometry analysis of DPSC' surface markers

The DPSC of P3 in T75 flasks were digested with 0.25% trypsin-EDTA, collected, and incubated for 30 min with monoclonal antibodies against human CD29, CD34, CD44, CD45, CD73, CD90, and CD105 (BD Pharmingen, USA; Abcam, USA), as well as isotype-matched control IgG1. CD44 and CD105 were labeled with phycoerythrin (PE). CD45 and CD90 were labeled with PE-CY5 conjugate. CD29, CD34, and CD73 were labeled with fluorescein isothiocyanate (FITC). The expression profiles for the cell surface markers were analyzed using a flow cytometer and Cell Quest software (Beckman Coulter, USA).

Colony forming unit assay

Using the low-density cell seeding method, the capacity of colony-forming units was assessed. DPSC (P3) were seeded at a density of 500 cells/well into 6-well plates (Corning Incorporated, Corning, NY, USA) and maintained in the normal growth medium. After 7 days, cells were fixed with 4% paraformaldehyde for 10 min, washed twice with PBS, and stained with crystal violet staining (Sigma, USA).

Multilineage differentiation of DPSC

Alizarin red staining: DPSC (P3) were seeded in 6-well culture plates at a density of 10^5 cells/well and cultured in α-MEM supplemented with 10% FBS and 1% of penicillin/streptomycin at 37˚C with 5% CO_2 in a humidified incubator. When the cells become 80% confluence, the culture medium was replaced with osteogenic medium (growth medium supplemented with 10 mM beta-glycerophosphate, 50 mg/L ascorbic acid, and 10 nM dexamethasone). The osteogenic medium was replenished every 3 days. At day 21, the cells were fixed with 4% paraformaldehyde for 20 min at room temperature and washed with PBS. Osteogenic cultures were stained with 2% alizarin red solution, pH 4.2 (500 µl/well, Sigma-Aldrich), for 5-10 min to assess for mineral nodule deposition detection by light microscopy.

Oil red O staining: DPSC (P3) were seeded in 6-well culture plates at a density of 10^5 cells/well and cultured in α-MEM supplemented with 10% FBS and 1% of penicillin/streptomycin at 37˚C with 5% CO_2 in a humidified incubator. When the cells become 90% confluence, the culture medium was replaced with adipogenic medium (growth medium containing 10 mg/L insulin, 1 µM dexamethasone, 0.5 mM 3-Isobutyl-1-methylxanthine and 0.2 mM indomethacin). The adipogenic medium was replenished every 3 days. At day 28, the cells were fixed with 4% paraformaldehyde for 30 min at room temperature and washed with PBS. Adipogenic cultures were stained with a working solution of the Oil Red O staining (Solarbio, China) for 30 min to observe the formation of intracellular lipid vacuoles by light microscopy.

Alcian blue staining: DPSC (P3) were resuspended in a growth medium at a density of 4×10^6 cells/ml. Ten microliters of this cell suspension containing 4×10^4 cells were pipetted in the center of each well of a 48-well plate (Corning Incorporated, Corning, NY, USA). Then, micro-masses were given 2 h to form. After

that, maintenance medium (0.5 ml/well) was added for 1 day, followed by the addition of chondrogenic medium (growth medium supplemented with 50 mg/L ascorbic acid, 0.1 μM dexamethasone, 40 mg/L L-Proline, 10 μg/L TGF-β3 and 1% Insulin-Transferrin-Selenium). The chondrogenic medium was refreshed every 3 days. At day 21, the micro-masses were fixed with 4% paraformaldehyde for 30 min at room temperature and washed with PBS. Chondrogenic cultures were stained with a working solution of Alcian blue staining (Solarbio, China) for 30 min to assess the chondrogenic differentiation.

Cell proliferation assay

To determine the effect of CBD on DPSC proliferation ability, we used cell counting kit-8 (CCK-8; Dojindo, Japan). DPSC were seeded at a density of 2×10^3 cells/well in 96-well plates (Corning Incorporated, Corning, NY, USA) in triplicate. After 24 h of culture, the old medium was replaced with the medium containing 0, 0.1, 0.5, 2.5, and 12.5 μM CBD (Sigma, USA) respectively (six repeats per concentration). The medium was replaced every 3 days. At 1, 3, or 5 days, the culture medium was discarded. Then, 90 μl medium and 10 μl CCK8 reagent was added to each well and incubated in the incubator at 37 ℃ for 1 h. The results were recorded by a microplate reader (Thermofisher, USA) at an absorbance of 450 nm.

Alkaline phosphatase (ALP) staining and activity

DPSC ($2 \times l0^4$ cells/well) were seeded in 48-well culture plates, and cultured in a complete medium for 24 h. Then, the old medium was replaced with the osteogenic medium containing 0, 0.1, 0.5, and 2.5 μM CBD respectively (four repeats per concentration). The medium was replenished every 3 days. On days 4 and 7, the original medium was removed. For ALP staining, the cells were fixed with 4% paraformaldehyde for 30 min. Then, the cells were washed twice with PBS and stained using the BCIP/NBT ALP color development kit (Beyotime, China). Staining was observed under a bright field microscope. (Leica, Germany).

For the measurement of ALP activity, the cells were washed twice with PBS, and lysate was extracted in a lysis buffer containing 0.1% Triton x-100. The total protein concentration in the cell lysate was analyzed by the BCA protein assay kit (Thermo Scientific, USA). The activity of ALP was performed using the ALP assay kit (Nanjing Jiancheng Chemical Industrial Ltd, China). The results were measured by a microplate reader at an absorbance of 520 nm. The value of ALP activity was normalized to total protein content.

Matrix mineralization assays

DPSC ($2 \times l0^4$ cells/well) were seeded in 48-well culture plates, and cultured in a complete medium for 24 h. Then, the old medium was replaced with the osteogenic medium containing 0, 0.1, 0.5, and 2.5 μM CBD respectively. The medium was replenished every 3 days. On day 21, the original medium was removed. The mineralized matrix was stained by alizarin red staining. For semiquantitative analysis of 150 μl of 10% cetylpyridinium chloride (CPC) solution (Sigma, USA), the solution was added to each well of 48-well culture plates to dissolve the mineralized nodules. The eluted liquid was transferred to the 96-well plates. The results were measured by a microplate reader at an absorbance of 562 nm.

Development of micro-spheroids and characterization

The polydimethylsiloxane (PDMS) master mold with 200 μm pillar diameter, 150 μm pillar height, and 100 μm gap between two neighboring pillars was fabricated and used to develop agarose gel microwells for micro-spheroids culture. The PDMS mold was sterilized with 75% alcohol or under an ultraviolet lamp for 30 min. Agarose gel (Baygene, China; 3% w/v, agarose/deionized water) was sterilized using an autoclave and poured onto a PDMS mold containing pillars with a diameter of 200 μm. After allowing the agarose to solidify, microwell inserts with an area of ≈1.8 cm^2 were punched out and inserted in 24-well plates. PBS (1 mL) was then added, and the wells were sterilized using a UV light for 30 min. Each 24-well insert contained ≈2000 microwells. To form a micro-spheroid structure, DPSC were trypsinized, and $5x10^5$ cells were diluted in 500 μL of serum-free chemically defined medium (icell bioscience, China) and seeded in 24-well plates. Around 250 cells homed in each well and self-aggregated to form micro-spheroid. Micro-spheroids were further cultured in a serum-free osteogenic medium with or without CBD (2.5 μM). After that, images of micro-spheroids were captured at each time point, and the medium was changed every 48 h. For mechanism-related rescue experiments, CBD-treated micro-spheroids were incubated with an additional 100 ng/ml recombinant dickkopf-related protein 1 (DKK1, Sino biological, China) for 7 days. The half medium was replaced with fresh conditioned medium containing DKK1 every 24 h.

Live/dead staining

Cell viability in microspheres was assessed qualitatively with the Live/Dead viability/cytotoxicity kit (Solarbio, China). Briefly, micro-spheroids were rinsed with PBS, where after they were incubated in $2×10^{-6}$ M Calcein-AM and $4×10^{-6}$ M Propidium Iodide for 30 min at 37 °C, 5% CO_2, and 95% humidity. Images of each stained micro-spheroids were captured on days 1, 3, 7, and 14 using confocal laser scanning microscopy (CLSM, Leica TCS SP8). Live cells stain green and dead cells stain red.

Staining for cytoskeleton

Micro-spheroids were fixed for 30 min at room temperature with 4% paraformaldehyde, rinsed with PBS, permeabilized for 30 min with PBS containing 0.5% triton X-100, and rinsed with PBS. Cell nucleus and F-actin distribution within micro-spheroids were visualized by staining with 4',6-diamidino-2-phenylindole (DAPI) (Solarbio, China) and 0.8 U/mL tetramethyl rhodamine isothiocynate (TRITC) conjugated Phalloidin (Solarbio, China) during 1 h at room temperature. Sequential images of the micro-spheroids were captured using a confocal laser scanning microscopy (CLSM, Leica TCS SP8) using respective filters. The Leica AF image processing software was used to construct 3D images.

RT-qPCR analysis

Total RNA was extracted from DPSC and micro-spheroids using an RNA isolation kit (Accurate Biotechnology, China). The total RNA (500 ng) from each sample was reverse-transcribed to cDNA (Accurate Biotechnology, Hunan, China). RT-qPCR was performed using an SYBR Green RT-qPCR kit

(Accurate Biotechnology, Hunan, China). The gene expressions of osteogenic markers alkaline phosphatase (ALP), bone morphogenetic protein 2 (BMP2), runt-related transcription factor 2 (RUNX2), osteopontin (OPN), osteocalcin (OCN), and WNT6 were analyzed by RT-qPCR. The data were normalized to the internal control GAPDH. The primer sequences used for RT-qPCR are listed in Table 1.

Western blotting

Pretreated DPSC and micro-spheroids were lysed with RIPA buffer (Beyotime, China) containing protease inhibitors (PMSF; Beyotime, China) on ice for 30 min. The cell lysate was centrifuged at 12,000 rpm for 15 min to collect the supernatant. Total protein concentration was measured using the BCA protein assay kit (Thermo Scientific, USA). Total protein (20 μg) was loaded in 10% SDS-PAGE gel (Epizyme, China) for protein separation and transferred into polyvinylidene fluoride (PVDF) membranes (Millipore, Billerica, MA, USA) using wet blotting techniques. The membrane was blocked with 5% nonfat milk powder for 1 h and washed thrice with TBST. The membrane was then incubated at 4℃ overnight with primary antibodies, which included rabbit anti-human Collagen I (COL-I, Abcam, England), rabbit anti-human RUNX2 (Abcam, England), rabbit anti-human WNT6 (Bioss, China), and rabbit anti-human β-catenin (Bioss, China). After incubation, the primary antibodies were removed. Horseradish peroxidase (HRP)-conjugated secondary antibodies (Abcam, England) was incubated at room temperature for 1 h. The protein bands were detected using an enhanced chemical luminescence kit (Beyotime, China). The ImageJ software was used for the semi-quantification of band intensity.

Mice calvarial bone defect repair

Animal experiments were conducted following the protocols approved by the Laboratory Animal Ethics Committee of Guangdong Huawei Testing Co., LTD in this study (No.20220103). Forty male athymic nude mice (Zhuhai BesTest Bio-Tech Co., Ltd., China), 6-8 weeks old and weighing 19-26g were used. Animals were housed at a specific pathogen-free animal facility in stable conditions (22 ± 2°C) with a 12 h dark/light cycle and ad libitum access to food and water. Animals were allowed to acclimatize for 1 week before experiments and were regularly monitored for signs of pain/infection, food intake, and activity during the entire experimental period.

Before implantation, both DPSC and micro-spheroids were cultured in an osteogenic medium with or without CBD for 2 weeks. Then, DPSC were digested with 0.25% trypsin-EDTA and the micro-spheroids were washed in PBS. After centrifugation at 1,000 rpm for 5 min, the supernatant was carefully removed and the cells were resuspended in 10% (w/v) GelMA hydrogels (EFL-GM-60; Engineering For Life, China) which were sterilized by filtering through a 0.22 μm syringe filter. Constructs (≈7.5×10^5 DPSC /3×10^3 micro-spheroids per construct, n=8) with a diameter of 3 mm and a depth of 1 mm were exposed to LAP 405 nm blue light (Engineering For Life, China) for 5 s as seen in Fig. 5A. Controls transplanted with 10% (w/v) GelMA hydrogel. The 40 cranial defects were randomly separated into 5 groups: (a) control, (b) DPSC, (c) CBD (2.5 μM)-treated DPSC, (d) micro-spheroids, and (e) CBD (2.5 μM)-treated micro-spheroids. DPSC and micro-spheroids entrapped within the microgel units were cultured at 37 °C with 5% CO_2 before

implantation. To assess cell viability, the Live/Dead staining assay was performed on the GelMA hydrogel constructs cultured in vitro for 1, 3, and 7 days.

Preoperatively, all animals were anesthetized by intramuscular injections of ketamine hydrochloride (35 mg/kg) and xylazine (5 mg/kg). Following anesthesia, the calvarial bone was exposed, and a 3 mm circular bone defect was created with a trephine drill under normal saline irrigation. Constructs were placed into the defect, and the skin was sutured to close the wound. The animals received antibiotic therapy for 3 days. After 8 weeks, the mice were sacrificed by isoflurane inhalation through the approved Ethics Committees' methods and calvarial bone was collected and fixed with 4% paraformaldehyde for subsequent micro-computed tomography (micro-CT) and histological analysis.

Micro-CT analysis

Micro-CT images were taken using micro-CT equipment (Skyscan-1172; Bruker, Kontich, Belgium). The X-ray source is set at 60 kV and 100 μA the three-dimensional image is obtained by isotropy with the voxel size of 10 μm. The serial sections were reconstructed into a 3D image using reconstructions and osteogenic parameters conducted with NRecon v.1.6.9 software. CTAn (Bruker micro-CT, BE) was used for all image processing and quantification of mineralized tissue. The percentage of mineralized tissue was calculated with respect to the total explant volume. Bone volume was measured by using a fixed threshold setting for all images. CTvox (Bruker micro-CT, BE) was used to create 3D visualization. The osteogenic parameters such as bone volume/total volume (BV/TV), bone surface/total volume (BS/TV), bone mineral density (BMD), and trabecular thickness (Tb. Th) were measured.

Histology and immunostaining analysis

For histological analysis, all samples were fixed, demineralized, dehydrated, and embedded in paraffin. The sample blocks were sectioned to a thickness of 4 μm and stained with hematoxylin and eosin (H&E) as well as Masson’s trichrome. The newly formed mineralized area was measured using ImageJ software.

Micro-spheroids were fixed with 4% paraformaldehyde at room temperature for 2 h and washed with PBS. After centrifugation at 500 rpm for 5 min, micro-spheroids were snap-frozen, embedded in optimal cutting temperature compound (OCT) compound, and sectioned on a cryostat at 5-μm thickness. After blocking with 1% bovine serum albumin (BSA; Sigma-Aldrich) for 1 h at room temperature, the frozen sections were incubated with the primary antibodies OCN (1:500; Proteintech, China) overnight. After a washing step with PBS, the secondary antibody was applied for 1 h (CoraLite488-conjugated Goat Anti-Rabbit IgG, 1:200; Proteintech, China). After nuclear staining with DAPI, sample imaging was performed with confocal laser scanning microscopy (CLSM, Leica TCS SP8). Immunofluorescence staining was quantified using ImageJ software from three different samples.

mRNA sequencing and bioinformatics analysis

The total RNA of DPSC and microspheres treated for 21 days with or without 2.5 μM CBD was extracted using Trizol® (Invitrogen, Carlsbad, CA). RNA samples were detected based on the A260/A280 absorbance ratio with a Nanodrop ND-2000 system (Thermo Scientific, USA), and the RIN of RNA was determined by an Agilent Bioanalyzer 4150 system (Agilent Technologies, CA, USA). Only qualified samples will be used for library construction. Paired-end libraries were prepared using an ABclonal mRNA-seq lib prep kit (ABclonal, China) following the manufacturer's instructions. PCR products were purified (AMPure XP system) and library quality was assessed on an Agilent Bioanalyzer 4150 system. Finally, the library preparations were sequenced on an MGISEQ-T7 and 150 bp paired-end reads were generated (Shanghai Applied Protein Technology, China). The data generated from the BGI platform were used for bioinformatics analysis. RNA-seq sequencing data quality was verified by Fastqc. Then clean reads were separately aligned to the reference genome with orientation mode using HISAT2 software to obtain mapped reads. FeatureCounts was used to count the reads numbers mapped to each gene. And then Fragments Per Kilobase per Million (FPKM) of each gene were calculated based on the length of the gene and the reads count mapped to this gene. Differential expression analysis for mRNA was performed using R package edgeR. Differentially expressed RNAs with $|\log2(FC)|$ value > 1 and q value < 0.05, considered as significantly modulated, were retained for further analysis.

Statistical analysis

All data were obtained from at least three independent experiments with each experiment in triplicate under identical conditions and shown as the mean ± standard deviation (SD). To test the significance of observed differences between the study groups, one-way analysis of variance (ANOVA) or Student's t-test of the GraphPad Prism Software (version 9.0, USA) was used. A value of $p < 0.05$ was considered a significant difference.

Results

Isolation and characterization of DPSC

DPSC start to crawl out from enzyme-digested dental pulp tissues after 5 days of culture. The cells around the tissue mass were adherent to the culture dish surface and proliferated gradually, forming the appearance of cell colonies (Fig. 1A). The DPSC showed fibroblast-like morphology and active proliferation capacity during passage 3 (Fig. 1B). DPSC were positive for MSC surface markers, including CD29, CD44, CD90, CD73, and CD105 and negative for hematopoietic cell markers, such as CD34, and CD45 (Fig. 1C). In addition, DPSC showed robust multilineage differentiation potential as indicated by osteogenic differentiation by alizarin red staining (Fig. 1D), adipogenic differentiation by Oil red O staining (Fig. 1E), and chondrogenic differentiation by Alcian blue staining (Fig. 1F). Lastly, DPSC presented apparent colony forming capacity at 7 days (Fig. 1G). These results imply the DPSC isolated in this study as a pure source of MSCs.

CBD (2.5 μM) promoted osteogenic differentiation of DPSC in vitro

CBD at concentrations of 0.1, 0.5, and 2.5 μM did not show cytotoxicity towards DPSC at days 1, 3, and 5 of culture. These concentrations of CBD even promoted DPSC proliferation on day 5. However, CBD at a concentration of 12.5 μM caused a significant decrease in cell viability on days 3 and 5, indicating the high dose-dependent cytotoxicity (Fig. 2A). CBD at concentrations of 0.1, 0.5, and 2.5 μM increased ALP production by DPSC at day 3 and 7 of culture. Among these 3 concentrations, CBD 2.5 μM showed the highest effect on ALP production at both time points. This result was also observed in the ALP activity of DPSC on day 7 (Fig. 2B and 2C). Moreover, CBD at concentrations of 0.1, 0.5, and 2.5 μM promoted matrix mineralization of DPSC at 21 days of culture as indicated by the alizarin red staining and quantification (Fig. 2D and 2E). Our results indicate 2.5 μM of CBD as an optimal dose for inducing the osteogenic potential of DPSC, and this dose was used for further experiments in this study.

Micro-spheroids development and characterization

The PDMS mold with uniform microwells is shown in Fig. 3A. The schematic presentation of agarose microwells on PDMS and the DPSC microspheres formation in microwells are shown in Fig. 3B and 3C. After successive induction during osteogenic medium with or without CBD, the cytoskeletal actin was stained with TRITC-labeled phalloidin and DAPI. The significant red fluorescent intensity indicated the compaction of micro-spheroids with actin cytoskeleton by the formation of dense stress fibers over time (Fig. 3D, Movie S1, S2 in Supporting Information). To assess cell viability, a Live/Dead viability assay was performed on DPSC micro-spheroids. Red fluorescence indicated dead cells, while green fluorescence indicated the presence of live cells. Although some dead cells were seen in the center of micro-spheroids, the majority of cells in the micro-spheroids were viable (Fig. 3E, Movie S3, S4 in Supporting Information). We also measured the diameter of micro-spheroids of DPSC during culture. The size of micro-spheroids decreased over time (Fig. 3F). Approximately 70 μm diameter of CBD-pretreated micro-spheroids with better cell survival were obtained at day 14.

CBD-pretreatment robustly induced osteogenic markers expression in micro-spheroids

Micro-spheroids showed robustly higher expression of BMP2, RUNX2, and OCN at day 7 compared with DPSC. CBD-treated DPSC or micro-spheroids showed an increasing trend in the expression of osteogenic markers ALP, BMP2, RUNX2, OPN, and OCN at day 7. Interestingly, CBD-treated micro-spheroids showed higher expression of BMP2, RUNX2, and OCN at day 7 compared with CBD-treated DPSC. Micro-spheroids showed an increasing trend in ALP, BMP2, RUNX2, OPN, and OCN expression at day 14 compared with DPSC. Similarly, CBD-treated DPSC also showed an increasing trend in ALP, BMP2, RUNX2, OPN, and OCN expression at day 14 compared with DPSC. CBD-treated micro-spheroids showed robustly higher expression of ALP, BMP2, OPN, and OCN at day 14 compared with micro-spheroids or CBD-treated DPSC. CBD-treated micro-spheroids also showed higher expression of RUNX2 at day 14 compared with CBD-treated DPSC (Fig. 4A and 4B). On day 14, Western blot analysis showed more protein expression of COL-I and RUNX2 in micro-spheroids compared with DPSC. CBD-treated micro-spheroids showed higher protein expression of COL-I and RUNX2 compared with CBD-treated DPSC. Meanwhile, CBD-treated micro-

spheroids also showed higher protein expression of COL-I compared with micro-spheroids. (Fig. 4C and 4D).

Immunofluorescence imaging and quantification showed higher expression of OCN in CBD-treated micro-spheroids compared with micro-spheroids at day 14 (Fig. 3E and 3F). Our results indicate a higher osteogenic potential of micro-spheroids than DPSC and CBD treatment in micro-spheroids further induces osteogenic potential compared with CBD treatment in DPSC.

CBD-pretreated micro-spheroids promoted bone regeneration in mice calvarial bone defects

We prepared DPSC and micro-spheroids loaded GelMA hydrogels construct for in vivo grafting. We evaluated gross views of the constructs with 7.5×10^5 DPSC or 3×10^3 micro-spheroids (Fig. 5B). The live/dead cell double staining assays showed that the majority of DPSC and micro-spheroids in GelMA hydrogels were viable at 1, 3 and 7 days. Similarly, DPSC in GelMA hydrogels gradually exhibit morphology with fibroblastic spindle shape at day 7 (Fig. 5C). Therefore, our results showed that GelMA hydrogel does not affect the viability of DPSC and micro-spheroids.

To investigate the effect of DPSC and micro-spheroids with or without CBD pretreatment on osteogenesis in vivo, we established a nude mouse calvarial defect model. Micro-CT images revealed incomplete healing after 8 weeks in the DPSC group. While CBD-treated DPSC and micro-spheroids groups significantly increased bone healing in the cranial defect model. In contrast, the CBD-treated micro-spheroids group further exhibited the most abundant bone formation, and small peninsulas of bone nodule formation along the margins of bone defect could be observed (Fig. 6A). In addition, quantification of micro-CT images (Fig. 6B) provided further evidence that bone volume/total volume (BV/TV), bone surface/total volume (BS/TV), bone mineral density (BMD), and trabecular thickness (Tb. Th) were the highest in the CBD-treated micro-spheroids group.

To assess whether CBD and micro-spheroids improved new bone formation, the calvarial bone specimens were histologically analyzed. HE staining showed that new bone formation was limited, and only minimal new bone formation around the margins of the native bone in the DPSC group and CBD-treated DPSC group, where soft fibrous tissue filled the center of the defect area. Whereas a moderate and abundant amount of new bone was observed in the micro-spheroids and CBD-treated micro-spheroids group, respectively (Fig. 6C). Furthermore, Masson’s trichrome staining revealed that CBD-treated micro-spheroids formed the greatest amount of osteoid, with woven/lamellar features in the defect area, as compared with the other groups at 8 weeks. Our results showed that CBD-treated micro-spheroids induce abundant mineralized bone tissue formation and promote DPSC-based bone defect healing.

Induced osteogenic potential of CBD-pretreated micro-spheroids was attributed to WNT6 upregulation

We conducted mRNA-seq on DPSC and micro-spheroids with or without CBD after successive osteogenic induction for 14 days. A pairwise comparison was implemented to determine the expression difference. Firstly, principal component analysis (PCA) showed data independence between the groups, indicating

the comparability of data (Fig. S1A). The volcano plots revealed a large number of differentially expressed genes (DEGs) between the DPSC and micro-spheroids with or without CBD (Fig. S1B). Micro-spheroids showed 1171 differentially upregulated and 861 differentially downregulated genes compared with DPSC. CBD-treated micro-spheroids showed 1513 differentially upregulated and 1454 differentially downregulated genes compared with CBD-treated DPSC. There were 1574 common DEGs during the analysis of overlapping DEGs in DPSC and micro-spheroids vs. CBD-treated DPSC (Fig. 7A). Kyoto Encyclopedia of Genes and Genomes (KEGG) pathway enrichment analysis of these 1574 common DEGs revealed that the majority of DEGs enriched to osteogenesis-related WNT signaling pathway (Fig. 7B). The heat map of WNT signaling related DEGs are shown Figure 7C. Among these genes, WNT6 was upregulated 10-fold in CBD-treated micro-spheroids compared with CBD-treated DPSC (Fig. 7D). β-catenin, the downstream signaling of WNT6, is a key pathway involved in osteogenesis. We validated the expression pattern of WNT6 and β-catenin in DPSC and micro-spheroids with or without CBD treatment by RT-qPCR and Western blot analysis. (Fig. 7E, 7F, and 7G).

DKK1, a pharmacological inhibitor of the Wnt/β-catenin pathway, inhibits β-catenin formation by binding to the low-density lipoprotein receptor-related protein 5/6 component of the WNT receptor complex. Thus, we incubate CBD-treated micro-spheroids with or without additional DKK1 to further confirm the role of WNT6 in the higher osteogenic potential of CBD-treated micro-spheroids. Western blot analysis showed that DKK1 significantly downregulated the expression of WNT6 and β-catenin in CBD-treated micro-spheroids. Moreover, DKK1 also decreased the protein expression of RUNX2 (Fig. 7H and 7I). These observations implied that CBD upregulates WNT6 in micro-spheroids that promote osteogenic potential via Wnt/β-catenin signaling.

Discussion

Cost-effective novel bone regeneration approaches are in urgent need for the effective repair of critical-sized bone defects. Although state-of-the-art stem cell therapy might be a potent tool for bone regeneration, the seed cell suspension cannot adequately represent the natural environment of stem cells in the body, such as tissue structure and cell-cell and cell-extracellular environment interactions (33). Many desired cellular characteristics are maintained or even promoted in stem cell-3D construct compared with traditional stem cell treatment approaches (15). CBD, a plant extract, has been reported to promote the osteogenic capacity of MSCs including DPSC (34). However, the osteoinductive effect of CBD on 3D-cultured MSCs has not been tested yet. This study developed self-assembled CBD-pretreated DPSC micro-spheroids which showed robust osteogenic potential in vitro and bone regenerative potential in vivo compared with CBD-pretreated DPSC. WNT6, a member of Wnt/β-catenin signaling was highly upregulated in the CBD-treated DPSC micro-spheroids compared with CBD-treated DPSC. Our results indicate that DPSC micro-spheroids can effectively transfer the osteogenic effect of in vitro pretreated CBD during orthotopic bone regeneration via upregulation of WNT6 (Fig. 8).

In this study, DPSC were obtained from the dental pulp of premolars extracted for orthodontics treatment without an additional invasion (4). We have further confirmed that DPSC have common features of MSCs

including colony formation and multilineage differentiation potential. A previous study reported that DPSC are characterized by a rapid proliferation rate, high clonogenic potential, and ability to differentiate into distinct cell lineages including odontoblasts, osteoblasts, chondrocytes, and others (35). In addition, DPSC have been proven to induce bone tissue regeneration in the calvarial bone defect model (36). Our results indicate that DPSC isolated in this study are highly pure MSCs and can be used as a source of seed cells for bone tissue engineering applications.

Shreds of literature have reported that CBD promotes the osteogenic differentiation of MSCs from different sources including DPSC (34, 37, 38). Some clinical studies have shown that CBD promotes the healing of non-infectious arthritis (39) and exerts a beneficial effect on bone metabolism (40). In the present study, we found that CBD at a concentration of 0.1-2.5 μM did not inhibit the viability of DPSC but at a concentration of 12.5 μM dramatically inhibited the viability of DPSC. CBD (2.5 μM) robustly promoted the osteogenic differentiation of DPSC. These results are in agreement with other studies that a low dose of CBD (<10 μM) enhances proliferation and osteogenic differentiation of MSCs (41-43), while the pro-mitotic effects weakened with a higher dose of CBD (>10 μM) (44-46). Based on our findings, we choose CBD (2.5 μM) as an optimal concentration to induce osteogenic potential in DPSC.

A 3D culture system is better to simulate the in situ microenvironments of cells and retain the original biological characteristics of stem cells (23, 33). DPSC cell aggregates successfully regenerate dental pulp in clinics but DPSC fail to do so (47). Based on these facts, we developed DPSC micro-spheroids for the first time using the micro-well culture technique as described previously (23). The DPSC micro-spheroids obtained from 250 cells/microwell were consistent in size (around 70 μm), round in shape, and injectable. Hydrogel-based stem cell spheroids are usually >100 μm in size that cause necrosis of cells present in the inner core of spheroids (48). Cell viability was maintained throughout the micro-spheroids during 2 weeks of in vitro culture and treatment of CBD. We believe that our developed micro-spheroids can be easily injected homogeneously in the microporous 3D-printed bone graft during the surgical procedure. This allows the homogeneous distribution of functional seed cells in large-size micro-porous bone grafts.

Developing stem cell micro-spheroids with highly osteogenic potential is still a challenge. In this study, DPSC micro-spheroids were cultured in presence of an osteogenic medium and CBD that robustly induces the osteogenic capacity of DPSC micro-spheroids. DPSC micro-spheroids showed higher expression of osteogenic differentiation markers in vitro compared with DPSC and CBD treatment further strengthens the osteogenic effect in micro-spheroids. A previous study had developed human periosteum stem cells derived from cartilaginous micro-spheroids to repair the critical-sized bone defect (23). Our study directly developed osteogenic micro-spheroids from DPSC for bone regeneration applications. Our culture system avoids the use of growth factors that reduces the cost and eliminates the possible adverse effects carried by micro-spheroids due to the effect of those growth factors (23).

Although MSCs showed robust osteogenic potential in vitro, these cells fail to regenerate bone during in vivo transplantation (3). This mainly occurs due to the poor viability of cells in avascular bone grafts (49). DPSC micro-spheroids grafted in bone defect showed higher bone regeneration potential

compared with DPSC. This outcome is in accordance with the results from the previous studies using cell aggregates or spheroid (23). Although the CBD-pretreated DPSC showed a better effect on bone regeneration compared to DPSC, this effect was not as pronounced as that of CBD-pretreated DPSC micro-spheroids. Our results indicate that CBD-pretreated micro-spheroids effectively transfer the in-vitro CBD pretreatment effect during orthotopic bone regeneration. Although BMP2 has a robust bone regenerative potential, it has certain adverse effects during in vivo applications including ectopic bone regeneration postoperative inflammation and associated adverse effects, ectopic bone formation, osteoclast-mediated bone resorption, inappropriate adipogenesis, and cervical spine swelling (50, 51). Therefore, our developed DPSC micro-spheroids can be used as a BMP2/other osteogenic drug's effect carrier without direct application of these drugs in vivo. Such an approach eliminates the in vivo adverse effect of the directly applied drugs and simplifies the clinical translation of various osteogenic drugs.

The Wnt/β-catenin pathway regulates the cell fate of MSCs differentiating to osteoblasts (52, 53). A previous study indicated that WNT6 significantly enhanced β-catenin activity during osteogenic differentiation (54, 55). CBD-mediated rescue of bone loss, oxidative stress, and inflammation are mainly attributed to the activation of the Wnt/β-catenin pathway (56, 57). In this study, we took advantage of RNA-Seq to explore the differentiation of mechanisms in DPSC and micro-spheroids with or without CBD treatment and found that WNT6 was a key component upregulated and responsible for higher osteogenic potential of CBD-pretreated micro-spheroids. Inhibition of WNT6 signaling by DKK1 reduced the osteogenic potential of CBD-pretreated micro-spheroids. These results indicate the key role of WNT6 in the induced osteogenic potential of CBD-pretreated micro-spheroids. However, the mechanism of CBD-induced WNT6 activation in DPSC micro-spheroids should be further investigated. This study developed a self-assembled CBD-pretreated osteogenic DPSC micro-spheroids with activated WNT6 which indicate a promising bone regeneration application in clinics.

In this study, spheroids culture could eliminate the direct in vivo use of osteogenic drugs during bone tissue engineering.

Declarations

Conflict of interest

The authors have read the journal's policy on disclosure of potential conflict of interest and declare that no conflict of interest exists.

References

1. Chan YH, Ho KN, Lee YC, Chou MJ, Lew WZ, Huang HM, et al. Melatonin enhances osteogenic differentiation of dental pulp mesenchymal stem cells by regulating MAPK pathways and promotes the efficiency of bone regeneration in calvarial bone defects. Stem Cell Res Ther. 2022;13(1):73.

2. Maroulakos M, Kamperos G, Tayebi L, Halazonetis D, Ren Y. Applications of 3D printing on craniofacial bone repair: A systematic review. J Dent. 2019;80:1-14.
3. Gugliandolo A, Fonticoli L, Trubiani O, Rajan TS, Marconi GD, Bramanti P, et al. Oral Bone Tissue Regeneration: Mesenchymal Stem Cells, Secretome, and Biomaterials. Int J Mol Sci. 2021;22(10).
4. Zhang W, Yelick PC. Tooth Repair and Regeneration: Potential of Dental Stem Cells. Trends Mol Med. 2021;27(5):501-11.
5. Kunimatsu R, Hiraki T, Rikitake K, Nakajima K, Putranti NAR, Abe T, et al. Effects of Human Deciduous Dental Pulp-Derived Mesenchymal Stem Cell-Derived Conditioned Medium on the Metabolism of HUVECs, Osteoblasts, and BMSCs. Cells. 2022;11(20).
6. Bacakova L, Zarubova J, Travnickova M, Musilkova J, Pajorova J, Slepicka P, et al. Stem cells: their source, potency and use in regenerative therapies with focus on adipose-derived stem cells - a review. Biotechnol Adv. 2018;36(4):1111-26.
7. Atlas Y, Gorin C, Novais A, Marchand MF, Chatzopoulou E, Lesieur J, et al. Microvascular maturation by mesenchymal stem cells in vitro improves blood perfusion in implanted tissue constructs. Biomaterials. 2021;268:120594.
8. Yang X, Ma Y, Guo W, Yang B, Tian W. Stem cells from human exfoliated deciduous teeth as an alternative cell source in bio-root regeneration. Theranostics. 2019;9(9):2694-711.
9. Gual-Vaques P, Polis-Yanes C, Estrugo-Devesa A, Ayuso-Montero R, Mari-Roig A, Lopez-Lopez J. Autogenous teeth used for bone grafting: A systematic review. Med Oral Patol Oral Cir Bucal. 2018;23(1):e112-e9.
10. Cen X, Pan X, Zhang B, Huang W, Pei F, Luo T, et al. miR-20a-5p contributes to osteogenic differentiation of human dental pulp stem cells by regulating BAMBI and activating the phosphorylation of Smad5 and p38. Stem Cell Res Ther. 2021;12(1):421.
11. Zheng C, Chen J, Liu S, Jin Y. Stem cell-based bone and dental regeneration: a view of microenvironmental modulation. Int J Oral Sci. 2019;11(3):23.
12. Walmsley GG, Ransom RC, Zielins ER, Leavitt T, Flacco JS, Hu MS, et al. Stem Cells in Bone Regeneration. Stem Cell Rev Rep. 2016;12(5):524-9.
13. Yuan Y, Zhang X, Zhan Y, Tang S, Deng P, Wang Z, et al. Adipose-derived stromal/stem cells are verified to be potential seed candidates for bio-root regeneration in three-dimensional culture. Stem Cell Res Ther. 2022;13(1):234.
14. Zhang S, Liu P, Chen L, Wang Y, Wang Z, Zhang B. The effects of spheroid formation of adipose-derived stem cells in a microgravity bioreactor on stemness properties and therapeutic potential. Biomaterials. 2015;41:15-25.
15. Jiang Z, Li N, Zhu D, Ren L, Shao Q, Yu K, et al. Genetically modified cell sheets in regenerative medicine and tissue engineering. Biomaterials. 2021;275:120908.
16. Futrega K, Atkinson K, Lott WB, Doran MR. Spheroid Coculture of Hematopoietic Stem/Progenitor Cells and Monolayer Expanded Mesenchymal Stem/Stromal Cells in Polydimethylsiloxane

Microwells Modestly Improves In Vitro Hematopoietic Stem/Progenitor Cell Expansion. Tissue Eng Part C Methods. 2017;23(4):200-18.

17. Xu H, Lyu X, Yi M, Zhao W, Song Y, Wu K. Organoid technology and applications in cancer research. J Hematol Oncol. 2018;11(1):116.
18. Bar-Ephraim YE, Kretzschmar K, Clevers H. Organoids in immunological research. Nat Rev Immunol. 2020;20(5):279-93.
19. Regmi S, Raut PK, Pathak S, Shrestha P, Park PH, Jeong JH. Enhanced viability and function of mesenchymal stromal cell spheroids is mediated via autophagy induction. Autophagy. 2021;17(10):2991-3010.
20. Cho S, Choi H, Jeong H, Kwon SY, Roh EJ, Jeong KH, et al. Preclinical Study of Human Bone Marrow-Derived Mesenchymal Stem Cells Using a 3-Dimensional Manufacturing Setting for Enhancing Spinal Fusion. Stem Cells Transl Med. 2022;11(10):1072-88.
21. Petrenko Y, Sykova E, Kubinova S. The therapeutic potential of three-dimensional multipotent mesenchymal stromal cell spheroids. Stem Cell Res Ther. 2017;8(1):94.
22. Zhang L, Yang G, Johnson BN, Jia X. Three-dimensional (3D) printed scaffold and material selection for bone repair. Acta Biomater. 2019;84:16-33.
23. Nilsson Hall G, Mendes LF, Gklava C, Geris L, Luyten FP, Papantoniou I. Developmentally Engineered Callus Organoid Bioassemblies Exhibit Predictive In Vivo Long Bone Healing. Adv Sci (Weinh). 2020;7(2):1902295.
24. Gao ZR, Feng YZ, Zhao YQ, Zhao J, Zhou YH, Ye Q, et al. Traditional Chinese medicine promotes bone regeneration in bone tissue engineering. Chin Med. 2022;17(1):86.
25. Zhang Y, Ma J, Zhang W. Berberine for bone regeneration: Therapeutic potential and molecular mechanisms. J Ethnopharmacol. 2021;277:114249.
26. Kogan NM, Melamed E, Wasserman E, Raphael B, Breuer A, Stok KS, et al. Cannabidiol, a Major Non-Psychotropic Cannabis Constituent Enhances Fracture Healing and Stimulates Lysyl Hydroxylase Activity in Osteoblasts. J Bone Miner Res. 2015;30(10):1905-13.
27. Blevins LK, Bach AP, Crawford RB, Zhou J, Henriquez JE, Rizzo MD, et al. Evaluation of the anti-inflammatory effects of selected cannabinoids and terpenes from Cannabis Sativa L employing human primary leukocytes. Food Chem Toxicol. 2022:113458.
28. Casares L, Garcia V, Garrido-Rodriguez M, Millan E, Collado JA, Garcia-Martin A, et al. Cannabidiol induces antioxidant pathways in keratinocytes by targeting BACH1. Redox Biol. 2020;28:101321.
29. Muthumalage T, Rahman I. Cannabidiol differentially regulates basal and LPS-induced inflammatory responses in macrophages, lung epithelial cells, and fibroblasts. Toxicol Appl Pharmacol. 2019;382:114713.
30. Qi X, Liu C, Li G, Luan H, Li S, Yang D, et al. Investigation of in vitro odonto/osteogenic capacity of cannabidiol on human dental pulp cell. J Dent. 2021;109:103673.

31. Volmar MNM, Cheng J, Alenezi H, Richter S, Haug A, Hassan Z, et al. Cannabidiol converts NF-kappaB into a tumor suppressor in glioblastoma with defined antioxidative properties. Neuro Oncol. 2021;23(11):1898-910.
32. Sarzi-Puttini P, Batticciotto A, Atzeni F, Bazzichi L, Di Franco M, Salaffi F, et al. Medical cannabis and cannabinoids in rheumatology: where are we now? Expert Rev Clin Immunol. 2019;15(10):1019-32.
33. Wu X, Su J, Wei J, Jiang N, Ge X. Recent Advances in Three-Dimensional Stem Cell Culture Systems and Applications. Stem Cells Int. 2021;2021:9477332.
34. Apostu D, Lucaciu O, Mester A, Benea H, Oltean-Dan D, Onisor F, et al. Cannabinoids and bone regeneration. Drug Metab Rev. 2019;51(1):65-75.
35. Nuti N, Corallo C, Chan BM, Ferrari M, Gerami-Naini B. Multipotent Differentiation of Human Dental Pulp Stem Cells: a Literature Review. Stem Cell Rev Rep. 2016;12(5):511-23.
36. Lee YC, Chan YH, Hsieh SC, Lew WZ, Feng SW. Comparing the Osteogenic Potentials and Bone Regeneration Capacities of Bone Marrow and Dental Pulp Mesenchymal Stem Cells in a Rabbit Calvarial Bone Defect Model. Int J Mol Sci. 2019;20(20).
37. Schmuhl E, Ramer R, Salamon A, Peters K, Hinz B. Increase of mesenchymal stem cell migration by cannabidiol via activation of p42/44 MAPK. Biochem Pharmacol. 2014;87(3):489-501.
38. Luo H, Rossi E, Saubamea B, Chasseigneaux S, Cochois V, Choublier N, et al. Cannabidiol Increases Proliferation, Migration, Tubulogenesis, and Integrity of Human Brain Endothelial Cells through TRPV2 Activation. Mol Pharm. 2019;16(3):1312-26.
39. Vela J, Dreyer L, Petersen KK, Arendt-Nielsen L, Duch KS, Kristensen S. Cannabidiol treatment in hand osteoarthritis and psoriatic arthritis: a randomized, double-blind, placebo-controlled trial. Pain. 2022;163(6):1206-14.
40. Heineman JT, Forster GL, Stephens KL, Cottler PS, Timko MP, DeGeorge BR, Jr. A Randomized Controlled Trial of Topical Cannabidiol for the Treatment of Thumb Basal Joint Arthritis. J Hand Surg Am. 2022;47(7):611-20.
41. Miller H, De Leo N, Badach J, Lin A, Williamson J, Bonawitz S, et al. Role of marijuana components on the regenerative ability of stem cells. Cell Biochem Funct. 2021;39(3):432-41.
42. Olivas-Aguirre M, Torres-Lopez L, Valle-Reyes JS, Hernandez-Cruz A, Pottosin I, Dobrovinskaya O. Cannabidiol directly targets mitochondria and disturbs calcium homeostasis in acute lymphoblastic leukemia. Cell Death Dis. 2019;10(10):779.
43. Kamali A, Oryan A, Hosseini S, Ghanian MH, Alizadeh M, Baghaban Eslaminejad M, et al. Cannabidiol-loaded microspheres incorporated into osteoconductive scaffold enhance mesenchymal stem cell recruitment and regeneration of critical-sized bone defects. Mater Sci Eng C Mater Biol Appl. 2019;101:64-75.
44. Solinas M, Massi P, Cantelmo AR, Cattaneo MG, Cammarota R, Bartolini D, et al. Cannabidiol inhibits angiogenesis by multiple mechanisms. Br J Pharmacol. 2012;167(6):1218-31.
45. Massi P, Vaccani A, Bianchessi S, Costa B, Macchi P, Parolaro D. The non-psychoactive cannabidiol triggers caspase activation and oxidative stress in human glioma cells. Cell Mol Life Sci.

2006;63(17):2057-66.
46. Nabissi M, Morelli MB, Amantini C, Liberati S, Santoni M, Ricci-Vitiani L, et al. Cannabidiol stimulates Aml-1a-dependent glial differentiation and inhibits glioma stem-like cells proliferation by inducing autophagy in a TRPV2-dependent manner. Int J Cancer. 2015;137(8):1855-69.
47. Xuan K, Li B, Guo H, Sun W, Kou X, He X, et al. Deciduous autologous tooth stem cells regenerate dental pulp after implantation into injured teeth. Sci Transl Med. 2018;10(455).
48. Itoh Y, Sasaki JI, Hashimoto M, Katata C, Hayashi M, Imazato S. Pulp Regeneration by 3-dimensional Dental Pulp Stem Cell Constructs. J Dent Res. 2018;97(10):1137-43.
49. Le H, Xu W, Zhuang X, Chang F, Wang Y, Ding J. Mesenchymal stem cells for cartilage regeneration. J Tissue Eng. 2020;11:2041731420943839.
50. James AW, LaChaud G, Shen J, Asatrian G, Nguyen V, Zhang X, et al. A Review of the Clinical Side Effects of Bone Morphogenetic Protein-2. Tissue Eng Part B Rev. 2016;22(4):284-97.
51. Nguyen V, Meyers CA, Yan N, Agarwal S, Levi B, James AW. BMP-2-induced bone formation and neural inflammation. J Orthop. 2017;14(2):252-6.
52. Zhang L, Tang Y, Zhu X, Tu T, Sui L, Han Q, et al. Overexpression of MiR-335-5p Promotes Bone Formation and Regeneration in Mice. J Bone Miner Res. 2017;32(12):2466-75.
53. Clevers H, Nusse R. Wnt/beta-catenin signaling and disease. Cell. 2012;149(6):1192-205.
54. Feng L, Zhang JF, Shi L, Yang ZM, Wu TY, Wang HX, et al. MicroRNA-378 Suppressed Osteogenesis of MSCs and Impaired Bone Formation via Inactivating Wnt/beta-Catenin Signaling. Mol Ther Nucleic Acids. 2020;21:1017-28.
55. Zheng M, Weng M, Zhang X, Li R, Tong Q, Chen Z. Beta-tricalcium phosphate promotes osteogenic differentiation of bone marrow-derived mesenchymal stem cells through macrophages. Biomed Mater. 2021;16(2):025005.
56. Vallee A, Vallee JN, Lecarpentier Y. Potential role of cannabidiol in Parkinson's disease by targeting the WNT/beta-catenin pathway, oxidative stress and inflammation. Aging (Albany NY). 2021;13(7):10796-813.
57. Li D, Lin Z, Meng Q, Wang K, Wu J, Yan H. Cannabidiol administration reduces sublesional cancellous bone loss in rats with severe spinal cord injury. Eur J Pharmacol. 2017;809:13-9.

Table

Table 1. Primers used in RT-qPCR to examine gene expression

Gene	Acc. No	Primer sequence (5’-3’)	Product length (bp)
ALP	NM_001127501.4	F: GGACCATTCCCACGTCTTCAC	137
		R: CCTTGTAGCCAGGCCCATTG	
BMP2	NM_001200.4	F: GGGAGAAGGAGGAGGCAAAGA	190
		R: CTGGGGAAGCAGCAACGCTA	
RUNX2	NM_001015051.4	F: ACCCAGAAGGCACAGACAGAAG	82
		R: AGGAATGCGCCCTAAATCACT	
OCN	NM_199173.5	F: CTCACACTCCTCGCCCTATTGG	147
		R: GTAGCGCCTGGGTCTCTTCACT	
OPN	NM_000582.2	F: GCTAAACCCTGACCCATC	72
		R: CTTTCGTTGGACTTACTTGG	
COL-I	NM_000088.4	F: CAGTGGTAGGTGATGTTCTGGGAG	150
		R: CAAGAGGCATGTCTGGTTCGG	
WNT6	NM_006522.4	F: GTGCAACTGCACAACAACGAGG	127
		R: GAAATGGAGGCAGCTTCTGCCA	
GAPDH	NM_001357943.2	F: GGACCTGACCTGCCGTCTAG	100
		R: GTAGCCCAGGATGCCCTTGA	

Figures

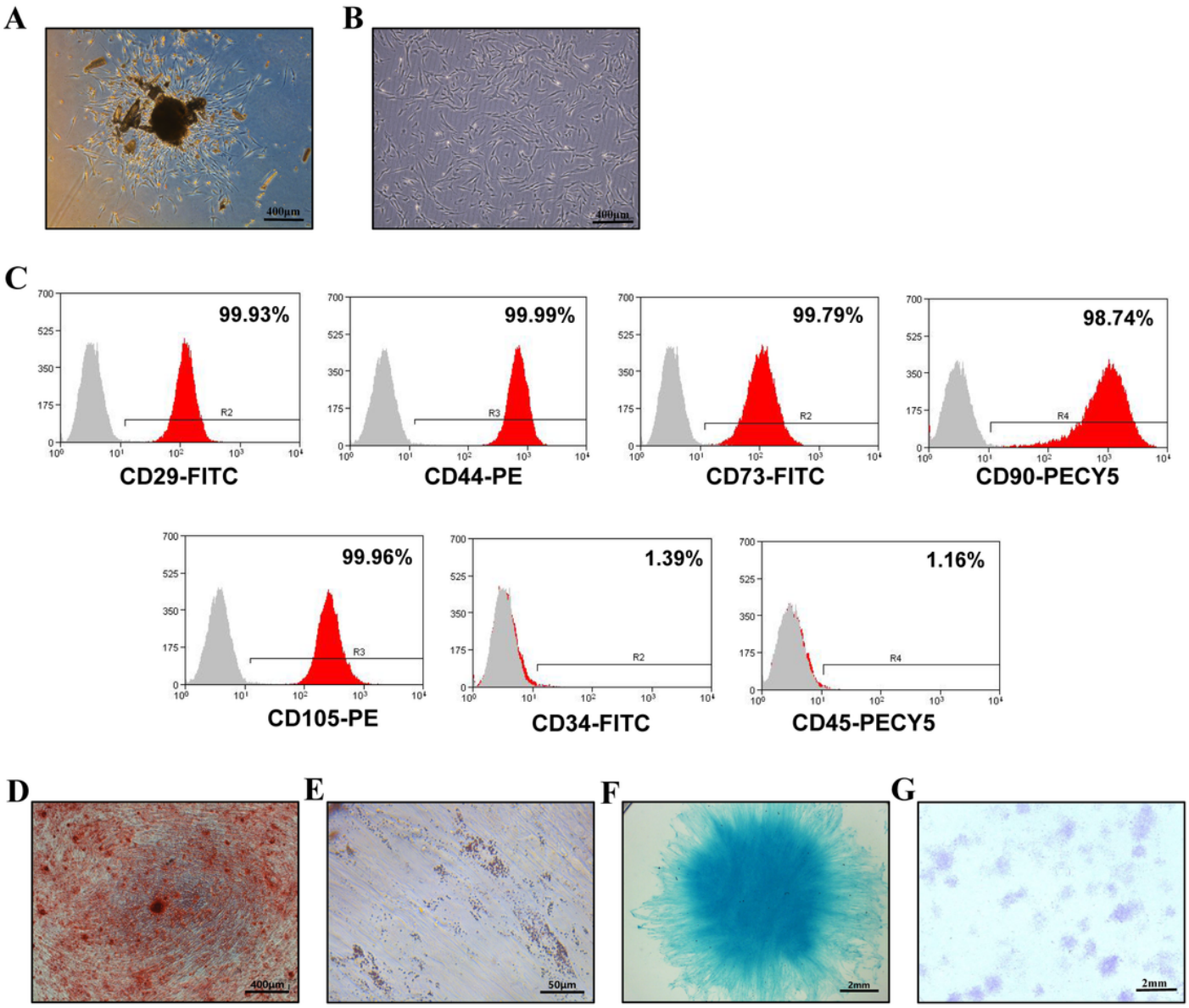

Figure 1

Characterization of DPSC. Primary stem cells from human permanent teeth P0: passage 0 (A) and P3: passage 3 (B). (C) Detection of cell surface markers in DPSC by flow cytometry. Analysis of osteogenic, adipogenic, and chondrogenic differentiation potential of DPSC using Alizarin red (D), Oil red O (E), and Alcian blue staining (F), respectively. (G) Crystal violet stained DPSC colonies at day 7 of colony formation assay.

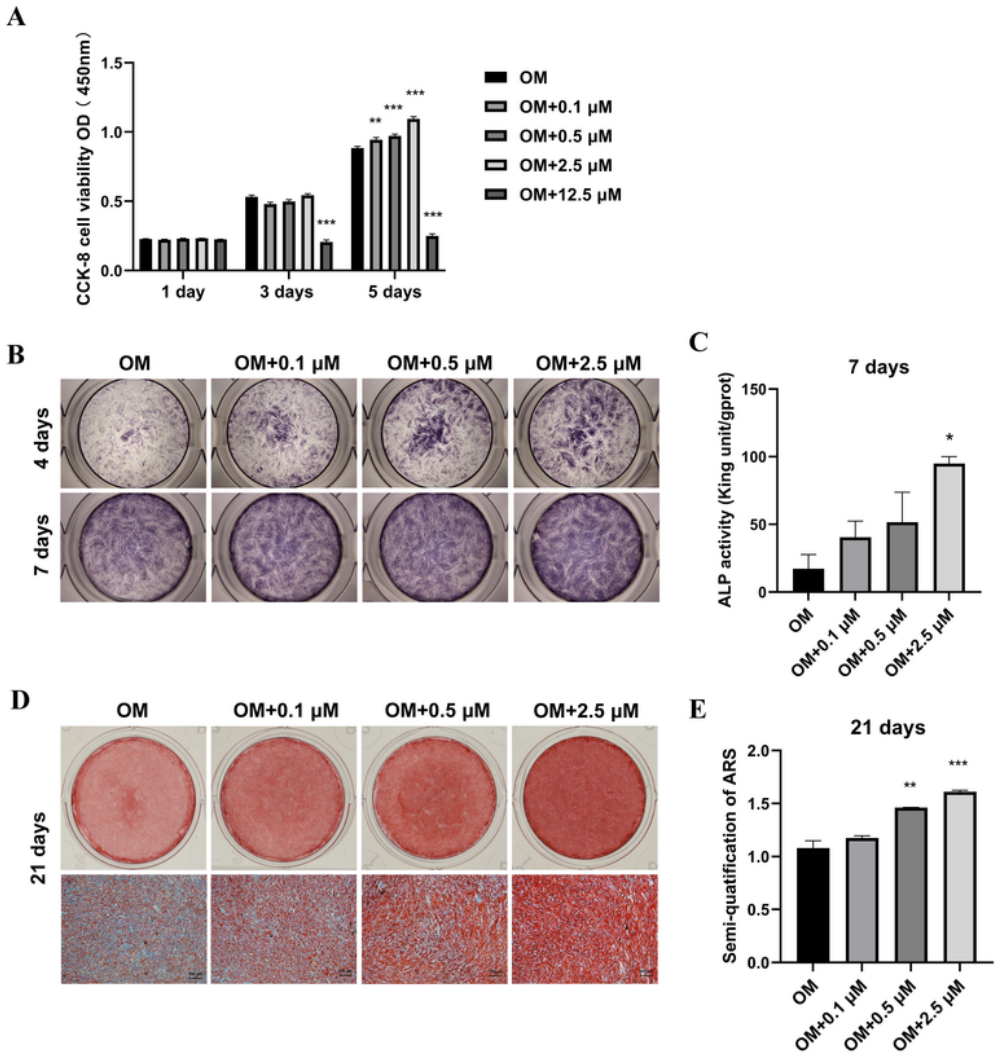

Figure 2

Effect of CBD on cell proliferation and osteogenic differentiation of DPSC in vitro. (A) Effect of 0.1, 0.5, 2.5, and 12.5 μM of CBD on the proliferation of DPSC (n = 6). ALP staining (B) and alizarin red staining (D) of DPSC cultured with CBD (0, 0.1, 0.5, and 2.5 μM). (C) ALP activity of DPSC cultured with CBD (n=4). (E) Quantification of mineralized matrix in DPSC cultured with CBD (n=4). The data are presented as

mean ± SD. Significant difference compared with the respective control group, *P<0.05, **P<0.01, and ***p < 0.001.

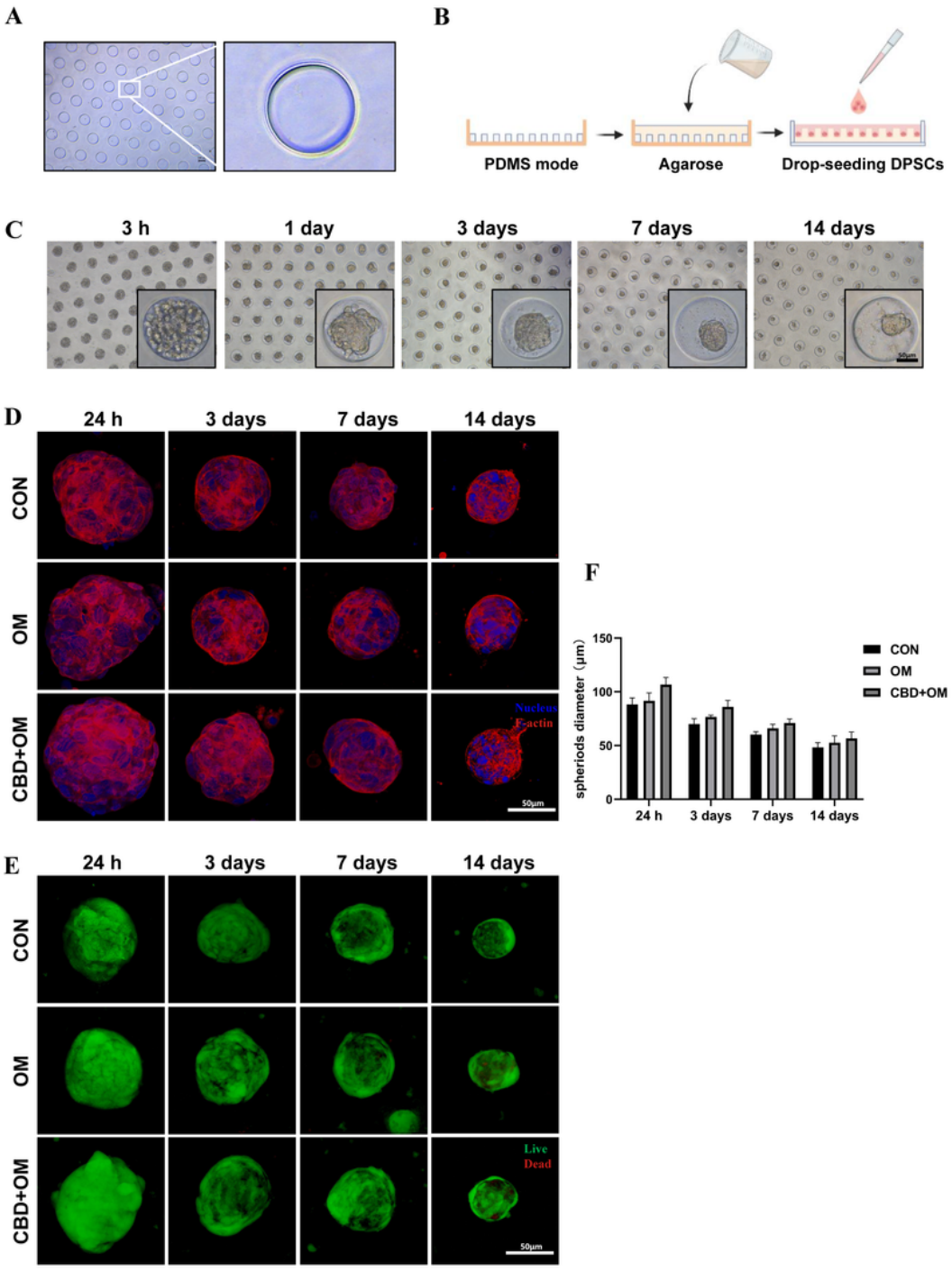

Figure 3

Micro-spheroids development in microwell method. (A) PDMS mold with uniform microwells. (B) The schematic presentation of agarose microwells on PDMS and the micro-spheroids formation in

microwells. (C) Representative bright-field images of DPSC to micro-spheroids in a time-dependent manner. Representative confocal z-projection images of cell cytoskeleton in micro-spheroids stained by Phalloidin actin (D), and Live/Dead cells in micro-spheroids stained by Calcein AM/PI (E). (F) The diameter of micro-spheroids over time. Scale bar 50 μm. The data are presented as mean ± SD (n=4).

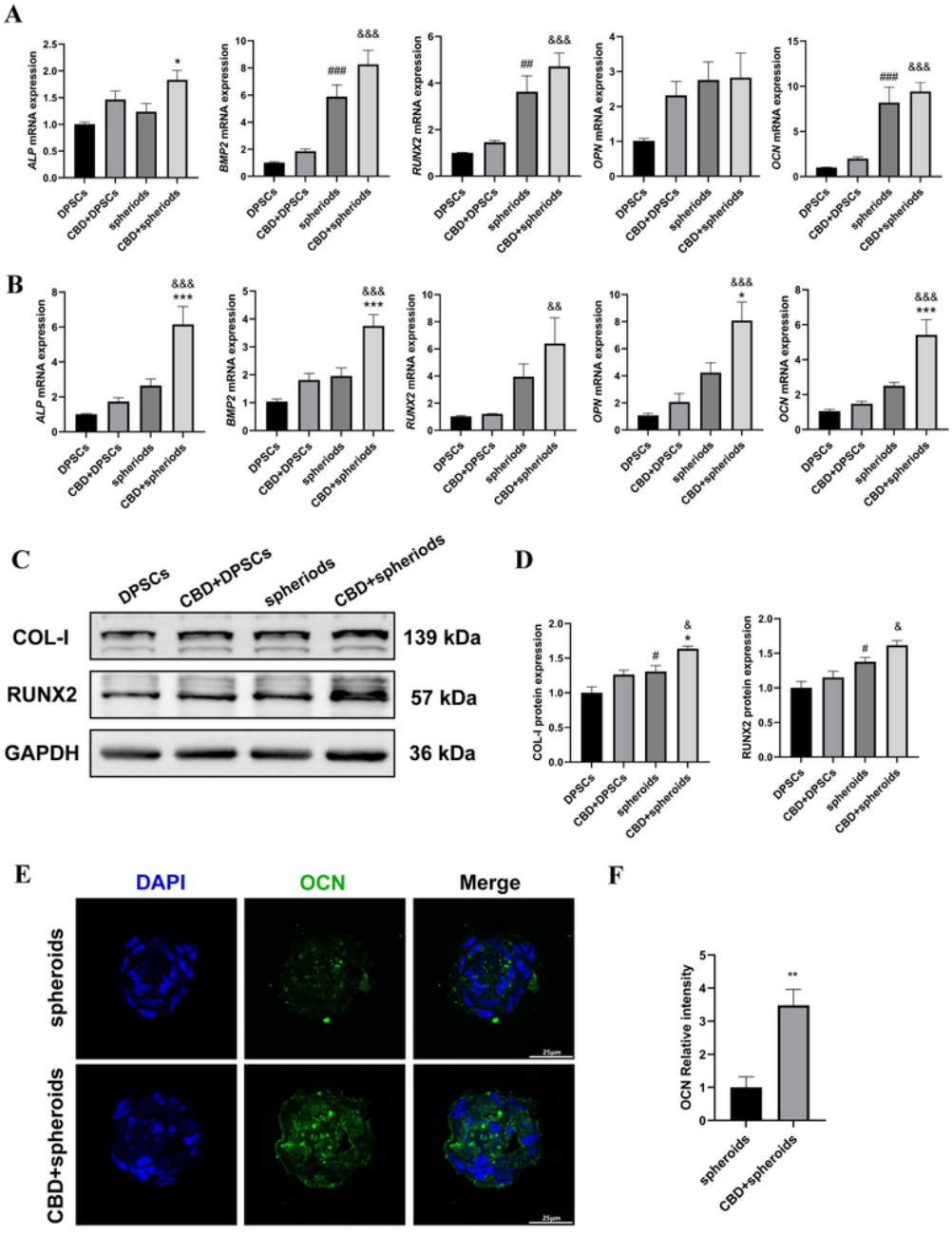

Figure 4

CBD (2.5 μM) induced osteogenic markers' expression in micro-spheroids. ALP, BMP2, RUNX2, OPN, and OCN mRNA expression at day 7 (A) and at day 14 (B). (C) Representative western blots of CoL-1 and RUNX2 expression at day 14 and quantification (D). (E) The images of the frozen sections obtained from micro-spheroids cultured at 14 days under osteogenic medium with or without CBD stained with immunofluorescence and (F) quantification. Data were presented as the mean ± SD (n=3). Significant difference compared between DPSC and spheroids groups, $^{\#}P<0.05$, $^{\#\#}P<0.01$, and $^{\#\#\#}p<0.001$; compared between spheroids and CBD+spheroids groups, *P<0.05, **P<0.01, and ***p<0.001; compared between CBD+DPSC and CBD+spheroids groups, $^{\&}P<0.05$, $^{\&\&}P<0.01$, and $^{\&\&\&}p<0.001$.

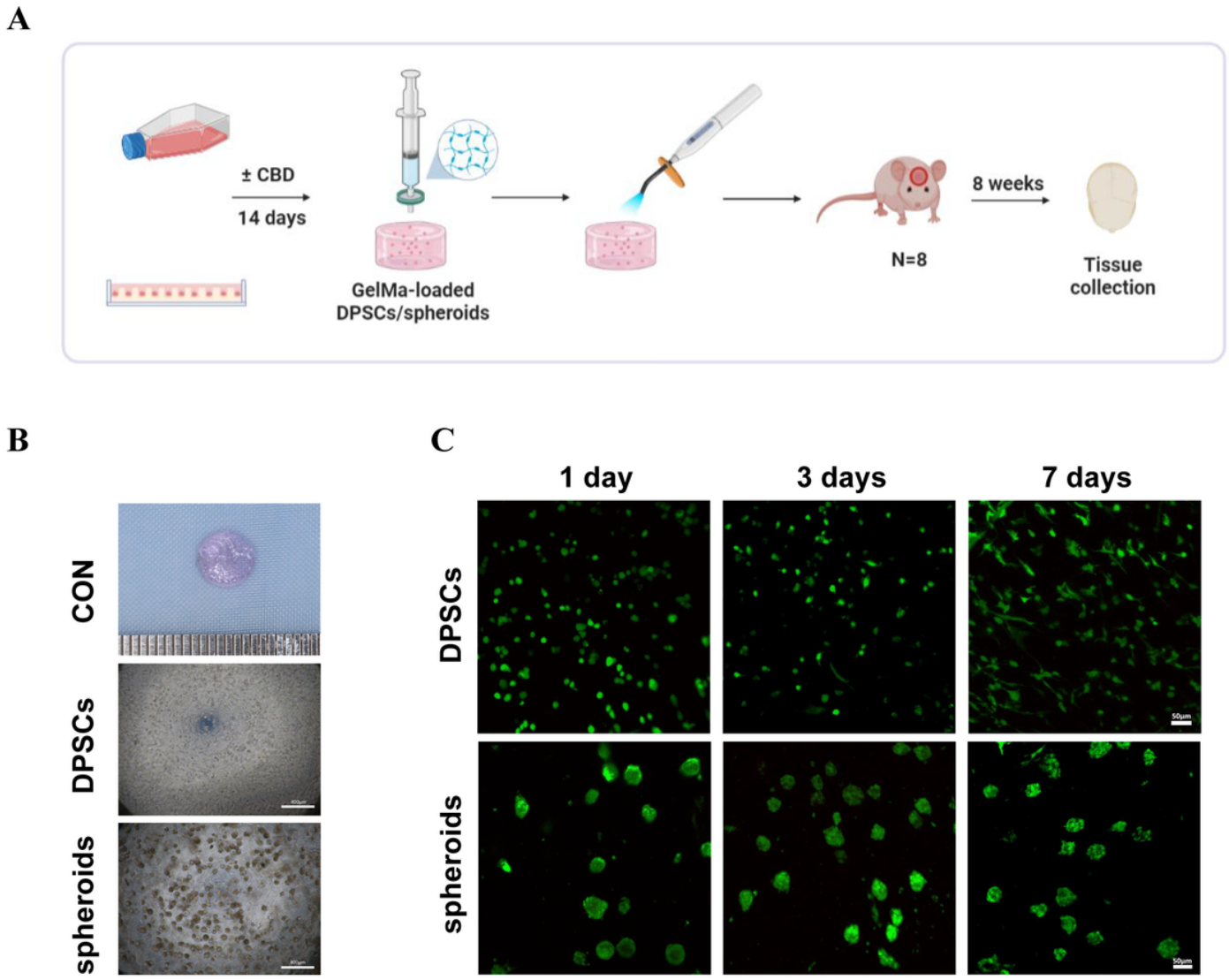

Figure 5

Preparation of DPSC or micro-spheroids loaded GelMA hydrogel constructs for in vivo grafting. The schematic illustration of cell-loaded GelMA hydrogels preparation in vitro and subsequent in vivo

construct grafted groups (A). (B) The images of the constructs of DPSC-loaded GelMA hydrogels and spheroids-loaded GelMA hydrogels. (C) Images of confocal microscopy showing DPSC or micro-spheroids viability in GelMA hydrogels assessed using Live/Dead assay.

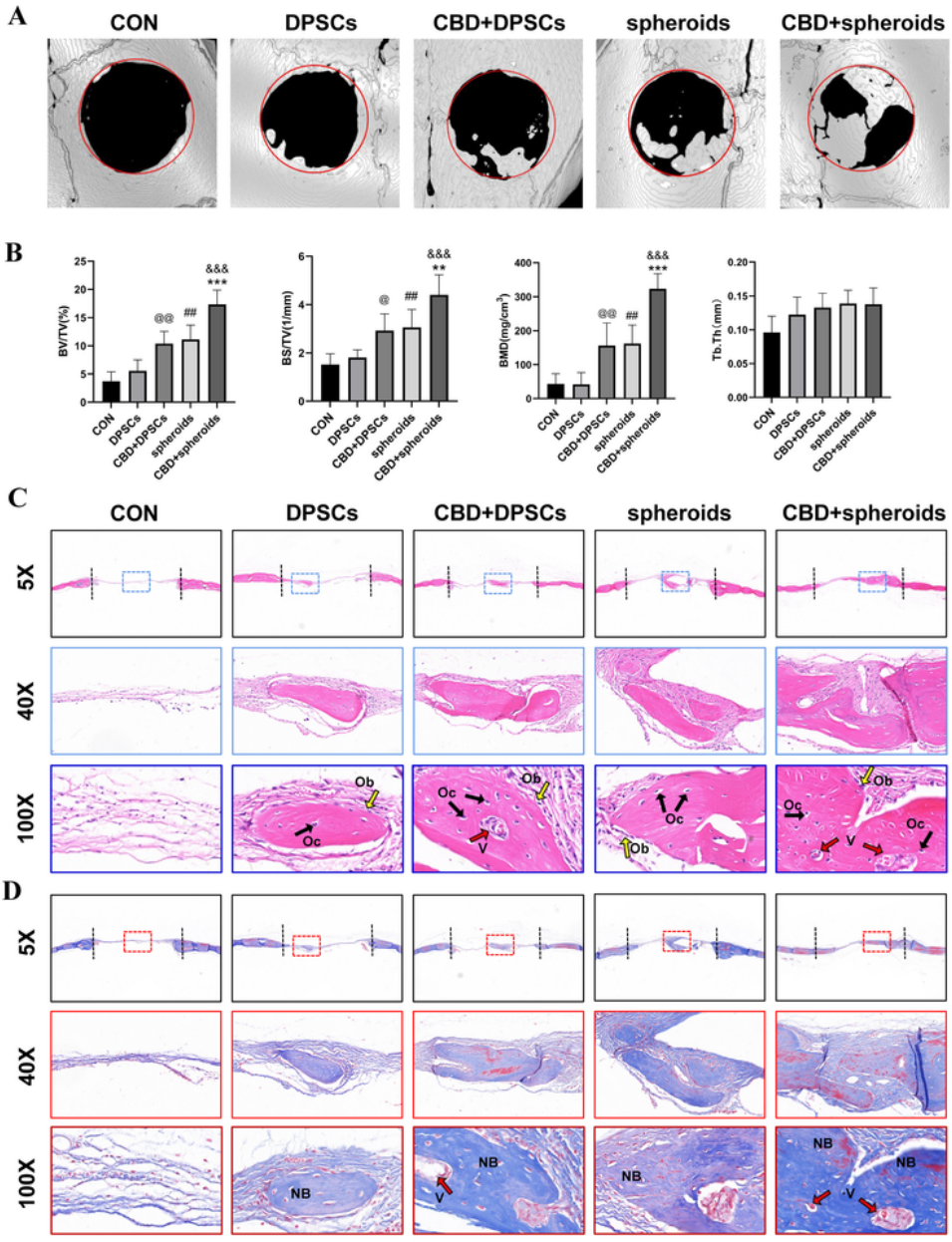

Figure 6

CBD-pretreated micro-spheroids promoted bone regeneration in mice calvarial bone defects. (A) Micro-CT images of calvarial bone defects after 8 weeks. (B) Quantitative analysis of newly formed bone parameters, bone volume/total volume (BV/TV), bone surface/total volume (BS/TV), bone mineral density (BMD), and trabecular thickness (Tb. Th) (n=8). Representative microscopic images of histological tissue sections: (C) HE staining and (D) Masson staining. Oc: osteocyte (black arrows); Ob: osteoblast (yellow arrows); NB: new bone; v: vessel (red arrows). Significant difference compared between DPSC and CBD+DPSC groups, $^{@}P<0.05$, and $^{@@}P<0.01$; compared between DPSC and spheroids groups, $^{\#\#}P<0.01$; compared between spheroids and CBD+spheroids groups, **P<0.01, and ***p<0.001; compared between CBD+DPSC and CBD+spheroids groups, $^{\&\&\&}p<0.001$.

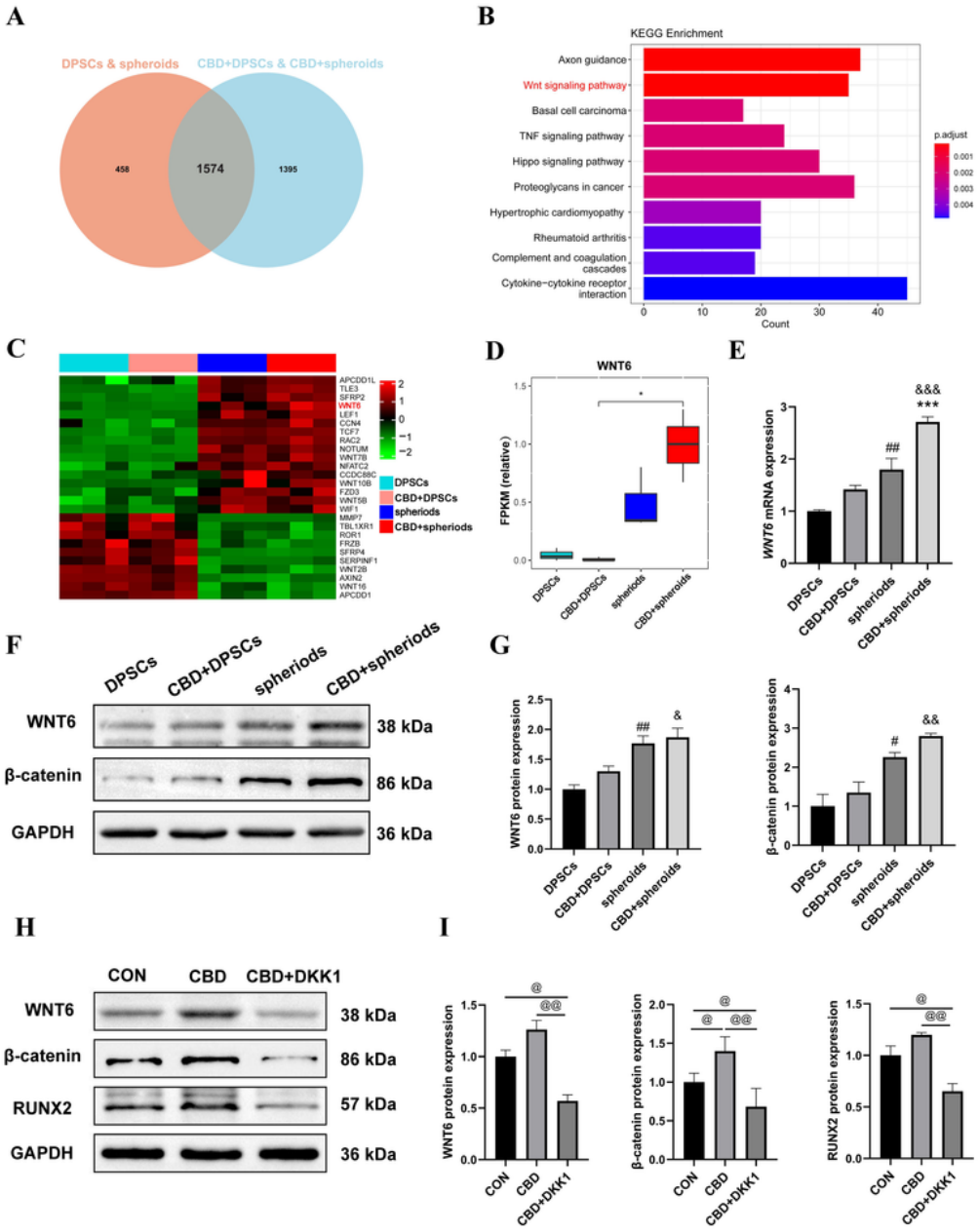

Figure 7

Transcriptomic analysis of DPSC and micro-spheroids with or without CBD treatment. (A) Venn diagram showing the differentially expressed genes (DGEs) between DPSC and micro-spheroids with or without CBD. (B) KEGG analysis of 1574 common DEGs. (C) Heat-map displaying the Wnt/β-catenin pathway-related DGEs between DPSC and micro-spheroids with or without CBD. (D) Quantification of differentially expressed WNT6 analyzed based on FPKM. (E) mRNA expression of WNT6. (F) Western blot analysis of

WNT6, β-catenin, and quantification (G). (H) Western blot analysis of the WNT6, β-catenin, and RUNX2 protein expression of micro-spheroids upon DKK1 treatment for 48 h and quantification (I). Data were presented as the mean ± SD (n=3). Significant difference compared between DPSC and spheroids groups, $^{\#}P<0.05$, and $^{\#\#}P<0.01$; compared between spheroids and CBD+spheroids groups, ***p<0.001; compared between CBD+DPSC and CBD+spheroids groups, $^{\&}P<0.05$, $^{\&\&}P<0.01$, and $^{\&\&\&}p<0.001$; compared between the two groups, $^{@}P<0.05$, and $^{@@}P<0.01$.

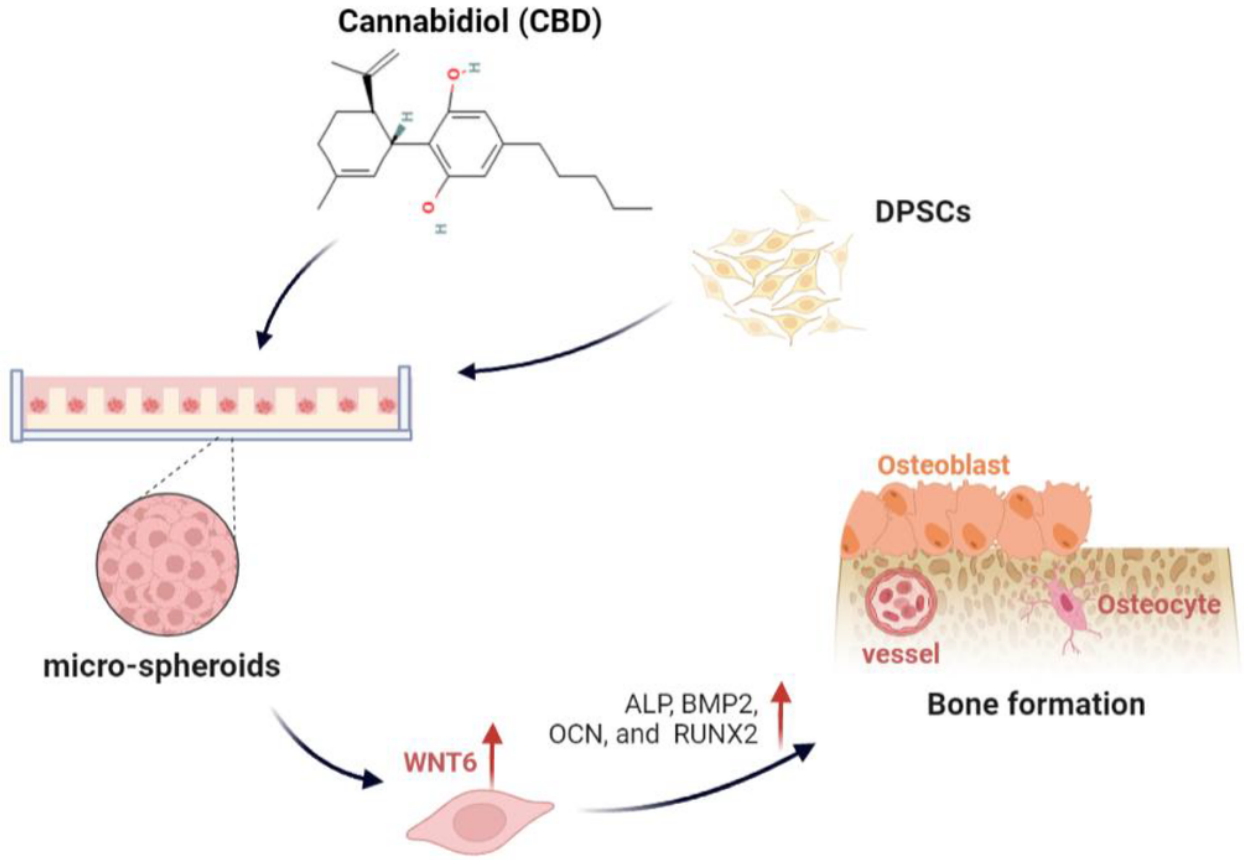

Figure 8

Schematic presentation of CBD-pretreated micro-spheroids and its osteogenic potential.

Supplementary Files

This is a list of supplementary files associated with this preprint. Click to download.

- Fig.S1.tif
- MovieS1.mp4
- MovieS2.mp4
- MoiveS3.mp4
- MoiveS4.mp4